From gut to brain: novel therapeutic strategies to combat obesity-associated cardiometabolic diseases

Li, Z.

CHAPTER 2

BUTYRATE REDUCES APPETITE AND ACTIVATES BROWN ADIPOSE TISSUE VIA THE GUT-BRAIN NEURAL CIRCUIT

Li Z, Yi CX, Katiraei S, Kooijman S, Zhou E, Chung CK, Gao Y, Van den Heuvel JK, Meijer OC, Berbée JFP, Heijink M, Giera M, Willems van Dijk K, Groen AK, Rensen PCN, Wang Y

***Gut 2018**, 67: 1269-1279*

Abstract

Objective: Butyrate exerts metabolic benefits in mice and humans, the underlying mechanisms being still unclear. We aimed to investigate the effect of butyrate on appetite and energy expenditure, and to what extent these two components contribute to the beneficial metabolic effects of butyrate.

Design: A cute effects of butyrate on appetite and its method of action were investigated in mice following an intragastric gavage or intravenous injection of butyrate. To study the contribution of satiety to the metabolic benefits of butyrate, mice were fed a high-fat diet with butyrate, and an additional pair-fed group was included. Mechanistic involvement of the gut-brain neural circuit was investigated in vagotomised mice.

Results: A cute oral, but not intravenous, butyrate administration decreased food intake, suppressed the activity of orexigenic neurons that express neuropeptide Y in the hypothalamus, and decreased neuronal activity within the nucleus tractus solitarius and dorsal vagal complex in the brainstem. Chronic butyrate supplementation prevented diet-induced obesity, hyperinsulinemia, hypertriglyceridemie and hepatic steatosis, largely attributed to a reduction in food intake. Butyrate also modestly promoted fat oxidation and activated brown adipose tissue (BAT), evident from increased utilization of plasma triglyceride-derived fatty acids. This effect was not due to the reduced food intake, but explained by an increased sympathetic outflow to BAT. Subdiaphragmatic vagotomy abolished the effects of butyrate on food intake as well as the stimulation of metabolic activity in BAT.

Conclusion: Butyrate acts on the gut-brain neural circuit to improve energy metabolism via reducing energy intake and enhancing fat oxidation by activating BAT.

Introduction

A positive energy balance, which occurs when energy intake exceeds energy expenditure, leads to the development of obesity. The prevalence of obesity has been increasing steadily over the past two decades, and obesity is becoming a global health concern. Obesity and obesity-initiated diseases are associated with high mortality and morbidity, mainly related to diabetes mellitus and cardiovascular disease [1]. Obese individuals have enhanced appetite [2] and/or reduced energy expenditure, mainly due to insufficient physical activity and impaired brown adipose tissue (BAT) activity [3, 4]. BAT contributes substantially to energy expenditure by combusting large amounts of triglycerides (TG) and glucose in humans (reviewed in refs) [5, 6], and its activity is mainly regulated through the sympathetic nervous system (SNS) under the control of the hypothalamus [7, 8]. The hypothalamus is also the central key regulator of food intake [9] and energy intake, receiving hormonal and neural signals emanating from the GI tract, adipose tissue and other peripheral organs. Although several pharmaceutical agents have been approved for the treatment of obesity, the clinical application of these agents for long-term body weight management is hampered due to the high incidence of adverse events [10]. The fundamental approach for combating against obesity is still lifestyle intervention, including diet adjustment.

Dietary fiber is deemed to be a key component in the healthy eating, mainly because dietary fiber is the main resource for production of endogenous short-chain fatty acids (SCFA) during bacterial fermentation in the colon. Interestingly, dietary supplementation of SCFAs has been shown to protect from obesity [11], making SCFAs promising candidates for the prevention of metabolic disorders. Of the SCFAs, in particular butyrate supplementation was found to have profound multiple metabolic benefits, including prevention of high-fat diet (HFD)-induced obesity, insulin resistance and hepatic steatosis [12-15]. A reasonable speculation is that butyrate acts on components of the energy balance, that is, stimulating energy expenditure, and/or reducing energy intake, thereby reducing obesity and obesity-associated disorders. A previous study indeed showed that butyrate induced peroxisome proliferator-activated receptor-γ coactivator-1α activity, thereby enhancing mitochondrial function in BAT and substantially promoting energy expenditure [13]. On the other hand, the effect of butyrate consumption on appetite is rather obscure. Whereas at least one study showed a clear reduction in food intake upon butyrate intervention [11], other studies reported that dietary supplementation of butyrate did not alter food intake [13, 15, 16] in diet-induced obese mice. Interestingly, clinical studies showed that dietary fiber, that is, oligofructose, increases endogenous butyrate production, accompanied by a reduction in energy intake [17, 18].

By using APOE*3-Leiden.CETP mice, a well-established translational model for developing human-like diet-induced obesity, dyslipidemia and metabolic syndrome [19, 20], we now aimed to evaluate the effect of butyrate on energy

intake and energy expenditure with respect to BAT activity, and to dissect the contribution of these two components of the energy balance to the metabolic benefits of butyrate. Here we provide first evidence that oral butyrate via the gut-brain neural circuit reduces appetite and activates BAT.

Materials and methods

Please see online supplementary materials and methods for an expanded version of this section.

Animals

APOE*3-Leiden.CETP (E3L.CETP) mice were obtained as previously described [21] and housed under standard conditions in conventional cages with free access to chow diet and water unless indicated otherwise. At the age of 10-12 weeks, male mice were used for experiments in accordance with the regulations of Dutch law on animal welfare.

Chronic intervention experiment

Mice received an HFD (60% kcal derived from lard fat and 0.25% cholesterol (w/w), Research Diets, New Brunswick, NJ) without (control group) or with 5% (w/w) sodium butyrate (Sigma Aldrich; butyrate group) for 9 weeks. Since butyrate was expected to reduce food intake, a third group of mice received the same amount of HFD as that of the butyrate group (pair-fed group).

Subdiaphragmatic vagotomy surgery

Mice received subdiaphragmatic vagotomy surgery [22] or sham surgery as controls. After a recovery period of 1 week after the surgery, mice received an HFD alone or supplemented with 5% (w/w) sodium butyrate for 7 weeks.

Statistical analysis

All data are expressed as mean ± SEM. For studies including three groups, differences between groups were determined using one-way analysis of variance test. When significant differences were found, Fisher's least significant difference test was used as a post hoc test to determine the differences between two independent groups. For studies including two groups, statistical differences between groups were calculated using a two-tail unpaired Student's t-test. A P value less than 0.05 was considered statistically significant.

Results

Oral rather than intravenous butyrate decreases food intake and inhibits orexigenic neuron activity in hypothalamus

We first evaluated the effect of butyrate on appetite. In overnight fasted mice, butyrate administration via intragastric gavage significantly prevented food intake within 1 hour after refeeding, and led to a 21% reduction in cumulative food intake over 24 hours (figure 1A). This acute reduction in food intake was accompanied with a large decrease in number of FOS-positive neurons within the arcuate nucleus in the hypothalamus (-73%, figure 1B). Furthermore, oral butyrate markedly decreased the portion of neuropeptide Y (NPY)-positive neurons that also express c-FOS (-49%, figure 1C), while did not influence the portion of pro-opiomelanocortin-positive neurons coexpressing c-FOS (figure 1D). In addition, oral butyrate clearly decreased the number of FOS-positive neurons within nucleus tractus solitarius (NTS) and dorsal vagal complex (DVC) in brainstem (-37%, figure 1E), without affecting the neuronal activity in either cortical region or hippocampal region (data not shown). Notably, 1 hour after gavage, oral butyrate supplementation raised the portal vein and peripheral circulating butyrate concentration as compared with the control group. To elucidate whether the increased circulating butyrate evoked the reduced appetite, we also administered butyrate directly into the circulation by intravenous injection. As a result, the circulating butyrate concentration markedly increased (online supplementary figure S1), however without influencing either acute refeeding or food intake within 24 hours (figure 1F). Collectively, these data imply that oral administration of butyrate reduces food intake and hypothalamic neuronal signaling independent of increased circulating butyrate levels, indicating a mechanism involving the gut-brain neural circuit.

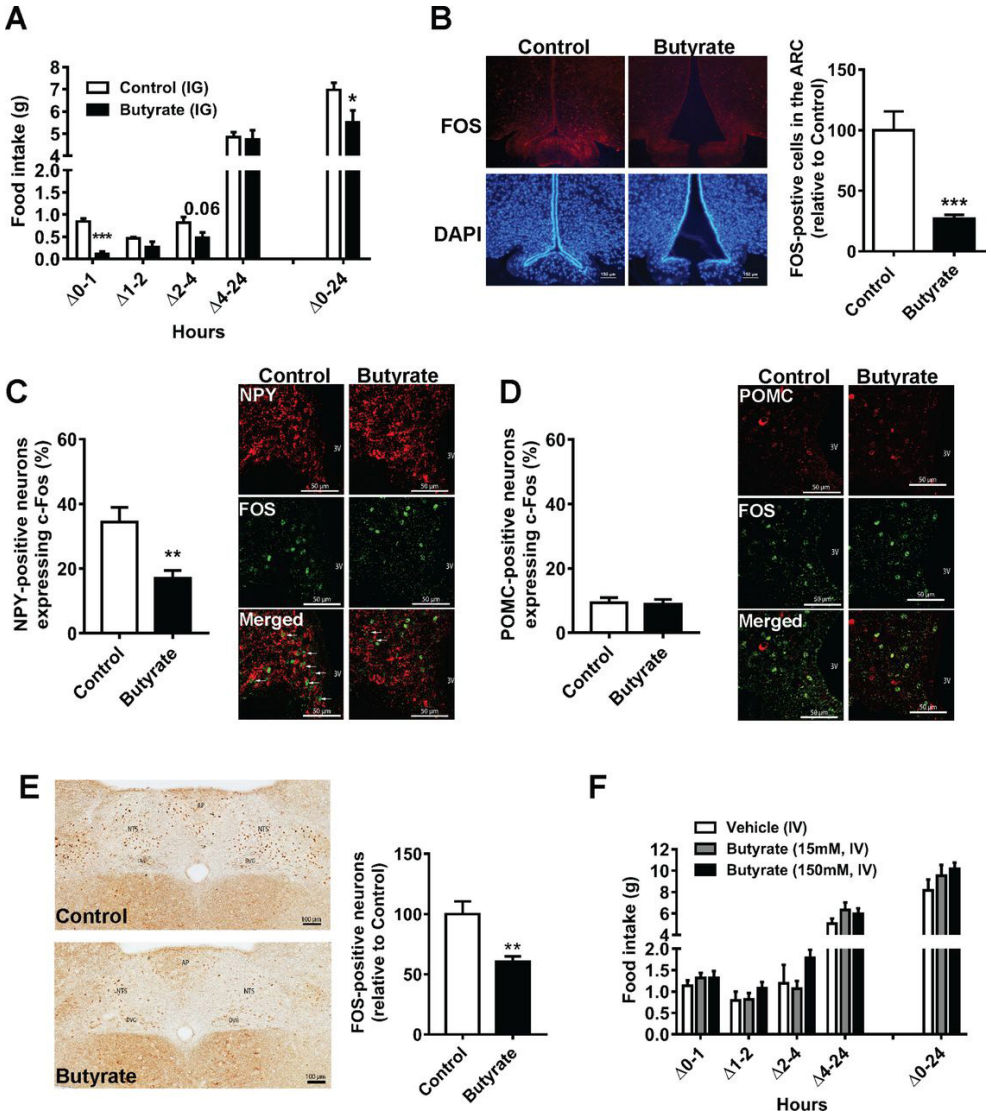

Figure 1. Oral but not intravenous butyrate decreases appetite and suppresses the activity of orexigenic neurons expressing NPY in the hypothalamus. After overnight fasting and randomization based on body weight, mice received vehicle or butyrate via the intragastric gavage (IG, A) or intravenous injection (IV, F). Food intake was measured during 24 hours. One hour after receiving butyrate IG, mice were anaesthetized and brains were collected immediately. FOS staining was performed in cryostat sections of frozen brains. The number of c-FOS-positive neurons within the arcuate nucleus in the hypothalamus (B) and nucleus tractus solitarius (NTS) and dorsal vagal complex (DVC) in the brainstem (E) was quantified. The colocalization percentages of NPY/c-FOS-positive neurons (C) and POMC/c-FOS-positive neurons (D) were quantified, with representative pictures as shown. Data are means ± SEM (n=8–9); *P<0.05, ***P<0.001 compared with control group. NPY, neuropeptide Y; POMC, pro-opiomelanocortin.

Butyrate consumption prevents HFD-induced obesity and hepatic steatosis, mainly via reducing food intake

To evaluate the contribution of reduced food intake to the metabolic benefits of chronic butyrate treatment, we fed E3L.CETP mice an HFD without or with sodium butyrate for 9 weeks, and included an additional group that was pair-fed to the butyrate group while receiving HFD. In line with the acute reduced appetite effect of a single oral butyrate administration, chronic dietary butyrate supplementation also caused a sustained reduction in food intake during the 9-week intervention period (figure 2A), resulting in 22% less food intake as compared with that of the control group (figure 2B).

We observed that butyrate completely prevented HFD-induced body weight gain (figure 2C), accompanied by decreased fat mass gain (figure 2D) without affecting lean mass as compared with the control group. Of note, during the first 7 weeks, food restriction per se by pair feeding diminished diet-induced obesity to a similar extent as observed by butyrate supplementation (figure 2C). After 9 weeks of intervention, as compared with control group, butyrate supplementation decreased body weight by -27% (figure 2E) and the weight of the gonadal (g) white adipose tissue (WAT) pad by -69% (figure 2F); while pair feeding decreased body weight by -18% (figure 2E) and the weight of the gWAT pad by -42% (figure 2F). This suggests that the antiobesity action of butyrate is largely dependent on reduction of food intake.

Butyrate also decreased liver weight (-25%, figure 2G), hepatic TG and phospholipid content (figure 2H) as compared with the HFD control group. Chronic butyrate consumption did not alter the levels of acetate, propionate and butyrate in peripheral blood, nor in portal vein blood (online supplementary figure S2). Pair-fed mice showed the same reduction in liver weight and lipid content as that of butyrate-treated mice (figure 2G, H). Representative pictures of liver sections confirmed that butyrate prevents HFD-induced hepatic steatosis through lowering of food intake (figure 2I).

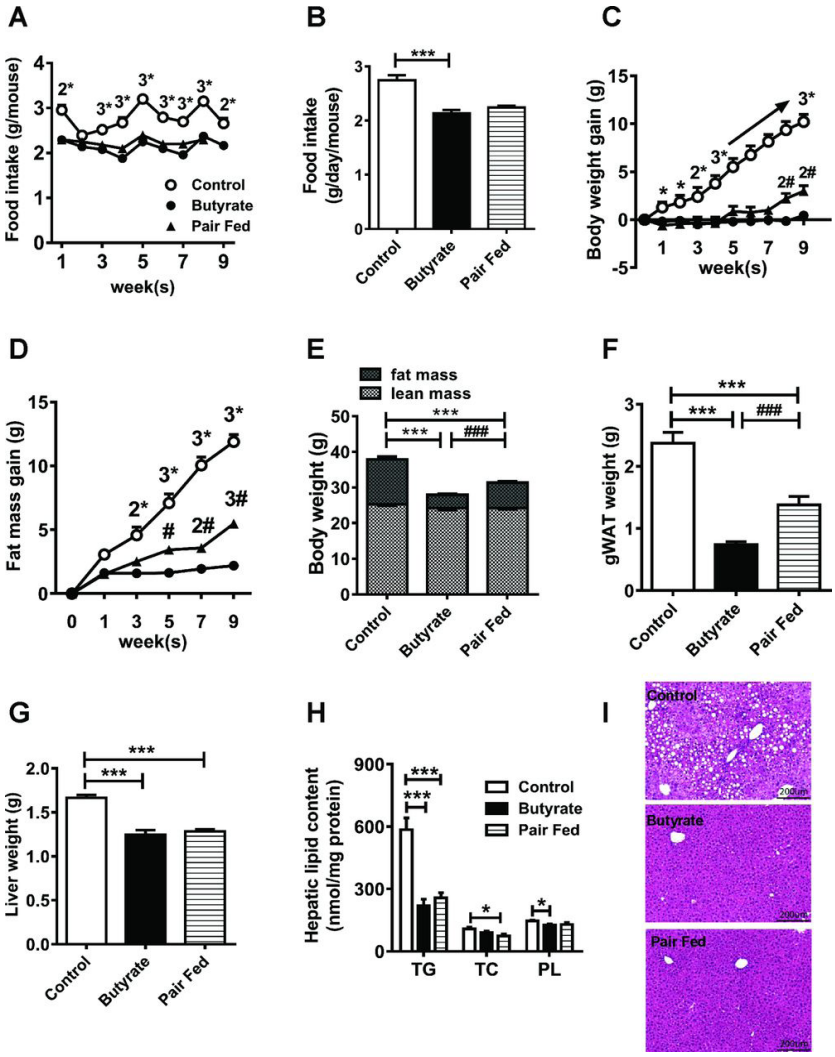

Figure 2. Butyrate consumption prevents high-fat diet (HFD)-induced obesity and hepatic steatosis, mainly via reducing food intake. Mice were individually housed and receive an HFD without (control group), or with 5% (w/w) sodium butyrate (butyrate group) for 9 weeks. A third group of mice received the same amount of HFD as consumed by the butyrate group (pair-fed group). Food intake was measured weekly (A), and average food intake per group through the whole intervention period was calculated (B). Body weight was measured weekly, and fat mass and lean mass were measured every other week by EchoMRI to calculate the body weight gain (C) and fat mass gain (D). At the end of this study, body composition (E), gonadal white fat pad weight (F), liver weight (G) and liver triglycerides (TG), total cholesterol (TC) and phospholipid (PL) content (H) were measured. Representative pictures of liver sections in H&E staining are shown (I). Data are means ± SEM (n=9–10); *P<0.05, **P<0.01, ***P<0.001 as control group compared with butyrate group; #P<0.05, ##P<0.01, ###P<0.001 as pair-fed group compared with butyrate group. gWAT, gonadal white adipose tissue.

Butyrate consumption improves lipid and glucose metabolism, in part by reduced food intake

Butyrate supplementation significantly decreased plasma TG levels (figure 3A), tended to decrease plasma glucose levels (P=0.05; figure 3B) and markedly decreased fasting insulin levels (figure 3C) and homeostatic model assessment of insulin resistance (figure 3D) as compared with controls, indicating that butyrate improves plasma lipid metabolism and insulin sensitivity. The beneficial effects of butyrate on plasma TG and glucose metabolism could be only partially attributed to the reduced food intake by butyrate, as pair feeding only reduced the plasma glucose level, and had no effects on plasma levels of TG and insulin (figure 3B).

To determine the organs involved in the TG and glucose lowering effects of butyrate, we injected mice with [^{3}H]TO-labelled TRL-like particles [23] and [^{14}C]DG. In parallel with a decreased plasma TG level, butyrate accelerated the clearance of [^{3}H]TO from the circulation as evidenced by reduced half-life of [^{3}H]TO (figure 3E). The accelerated [^{3}H]TO clearance was caused by a large increase in the uptake of [^{3}H]TO-derived activity by BAT depots (+174% for interscapular BAT (iBAT) and +123% for subscapular BAT; figure 3F), and to some extent by muscle and WAT (figure 3F). In contrast, food restriction *per se* by pair feeding did not increase the uptake of [^{3}H]TO-derived activity by BAT, muscle and WAT as compared with the control group. As may be expected, both butyrate treatment and pair feeding reduced the half-life of [^{14}C]DG (figure 3G) as compared with control group, indicating that butyrate accelerates the clearance of circulating [^{14}C]DG and could be explained by the reduction of food intake. Indeed, pair feeding increased the uptake of [^{14}C]DG by muscle and WAT to the same extent as that of butyrate treatment.

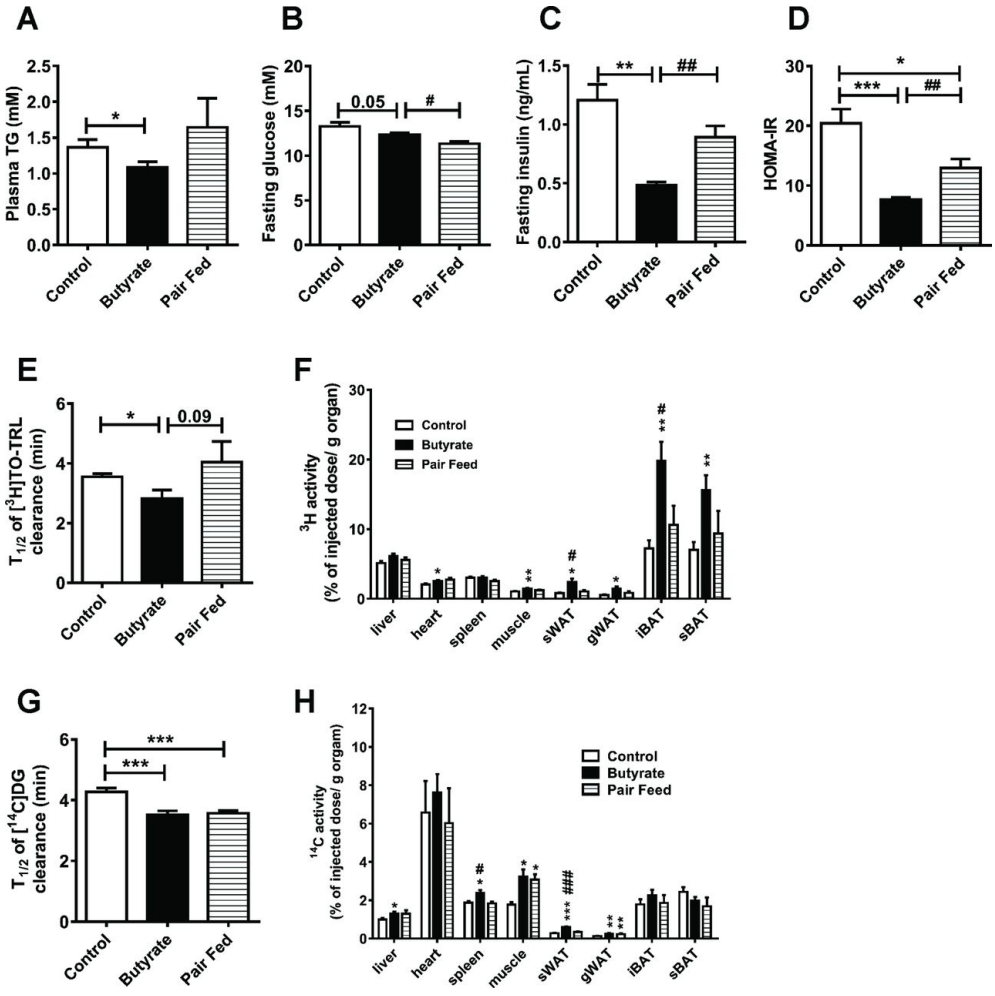

Figure 3. Butyrate consumption improves lipid and glucose metabolism, partially by reducing food intake. After 9 weeks of treatment with butyrate, plasma was assayed for TG (A), glucose (B) and insulin (C), and homeostatic model assessment of insulin resistance (HOMA-IR) (D) was calculated. At the end of this study, a combined TG and glucose clearance test was performed. Conscious mice were intravenously injected with [^{3}H]TO-labelled TRL-like particles and [^{14}C]DG. Subsequently, the plasma half-life of [^{3}H]TO (E) and [^{14}C]DG (G) was calculated, and 15 min after injection, the uptake of ^{3}H (F) and ^{14}C (H) by various tissues was assessed. Data are means±SEM (n=8–9); *P<0.05, **P<0.01, ***P<0.001 as control group compared with butyrate group; #P<0.05, ##P<0.01, ###P<0.001 as pair-fed group compared with butyrate group. gWAT, gonadal white adipose tissue; iBAT, interscapular brown adipose tissue; sBAT, subscapular brown adipose tissue; sWAT, subcutaneous white adipose tissue; TG, triglyceride.

Butyrate consumption promotes fat oxidation at the expense of carbohydrate oxidation

Since the effects of butyrate on body fat and lipid metabolism could only be partly attributed to reduction of food intake, indirect calorimetry was performed to determine the effects of butyrate on energy expenditure. In the first week of the intervention, when body weight of the mice was still comparable between the butyrate and control groups, mice were housed in fully automated metabolic cages. Butyrate treatment did not affect the spontaneous physical activity of the mice (figure 4A). Although no effect on total energy metabolism was detected (figure 4B), butyrate significantly decreased the respiratory exchange ratio during daytime (figure 4C). This was reflected by an increase in fat oxidation (figure 4D), mostly at the expense of carbohydrate oxidation (figure 4E) during daytime.

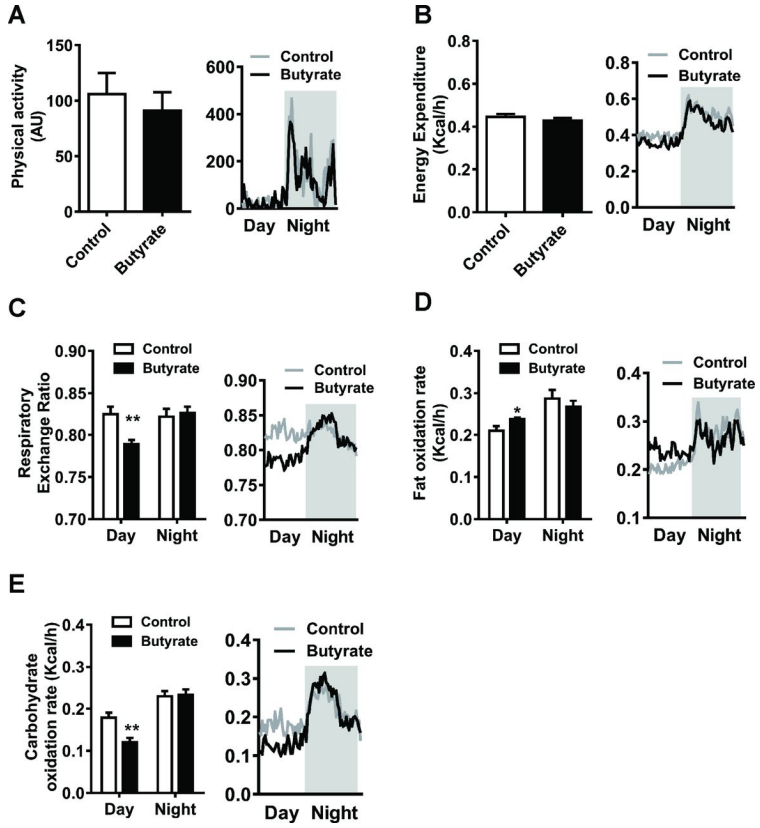

Figure 4. Butyrate promotes fat oxidation at the expense of carbohydrate oxidation. In the first week of the intervention, mice were housed in fully automated metabolic cages, and physical activity (A), energy expenditure (B) and respiratory exchange ratio (C) were monitored. Fat oxidation rate (D) and carbohydrate oxidation rate (E) were calculated. For bar graphs, data are shown as means ± SEM (n=7-8); for line graphs, data are shown as the mean for each group (n=7-8) during a 24-hour cycle (07:00–07:00).

Butyrate consumption increases BAT thermogenic capacity and sympathetic outflow towards BAT

Next we followed up on the stimulating effect of butyrate on [^{3}H]TO uptake by BAT and fat oxidation by studying BAT in more detail. Butyrate markedly decreased the weight of the iBAT pad (figure 5A), accompanied by a decrease in intracellular lipid vacuole content as compared with the control mice (figure 5B, E). The protein content of uncoupling protein (UCP)-1 per area of BAT was increased (figure 5C, E), suggesting increased thermogenic capacity of BAT. Furthermore, butyrate increased sympathetic outflow towards BAT, as evidenced by increased protein expression of tyrosine hydroxylase (TH), a marker of sympathetic nerve activity (figure 5D, E). As compared with the pair-fed group, butyrate-treated mice still showed reduced iBAT pad weight (figure 5A), intracellular lipid content (figure 5B) and increased UCP-1 protein content (figure 5C), suggesting butyrate consumption improves BAT thermogenic capacity only partly via a reduction in food intake.

In both subcutaneous WAT and gWAT, butyrate did not induce mRNA expression of the beige adipocyte markers Ucp-1 and Cidea (online supplementary figure S3A, B). Furthermore, we could not detect any UCP-1 protein expression in either WAT depot, suggesting that butyrate treatment does not induce browning of WAT.

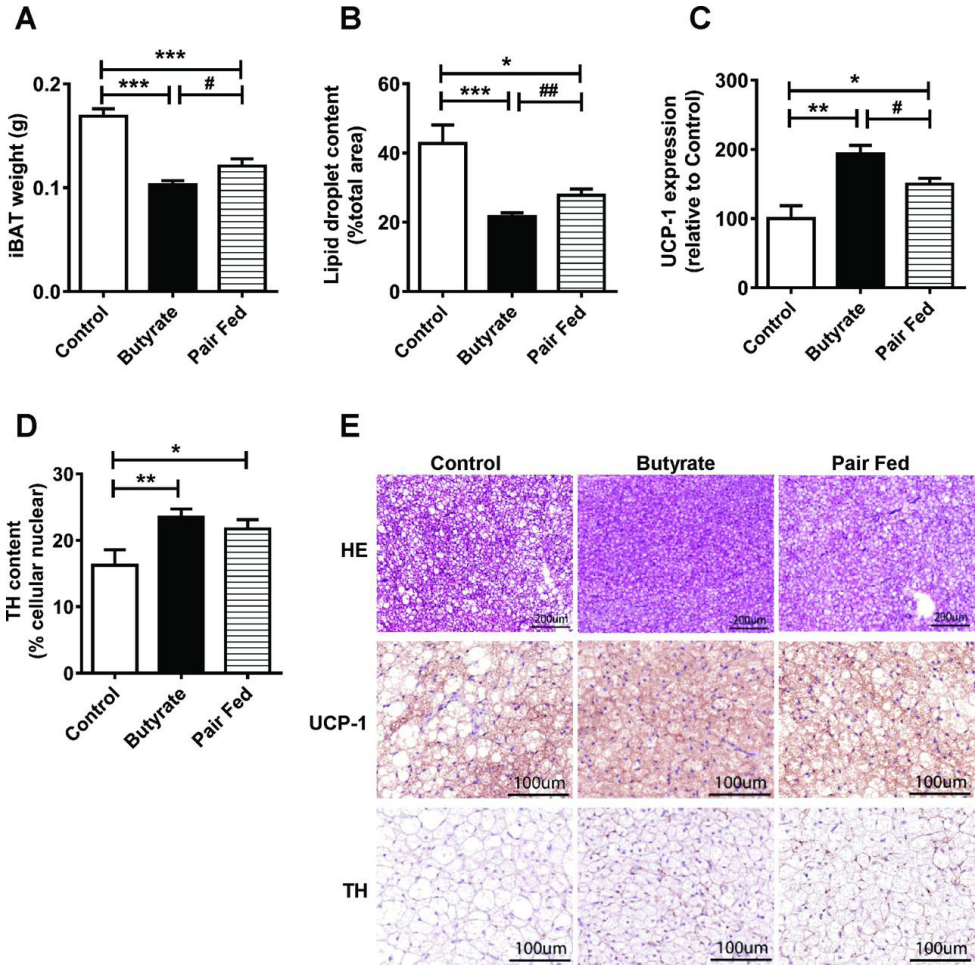

Figure 5. Butyrate increases brown adipose tissue (BAT) thermogenic capacity and sympathetic outflow towards BAT. After 9 weeks of intervention, the interscapular BAT (iBAT) pad was weighed (A) and sectioned. The lipid content within the iBAT was quantified after H&E staining (B). After immunostaining, the expression of UCP-1 (C) and TH (D) in iBAT was quantified with representative pictures shown (E). Data are means ± SEM (n=8–9); *P<0.05, **P<0.01, ***P<0.001 as control group compared with butyrate group; #P<0.05, ##P<0.01 as pair-fed group compared with butyrate group. TH, tyrosine hydroxylase; UCP, uncoupling protein.

The gut-brain neural circuit is necessary for the butyrate-induced satiety and BAT activation

To further investigate the mechanistic involvement of the gut-brain neural circuit in the beneficial effects of butyrate on energy metabolism, we performed the subdiaphragmatic vagotomy and sham surgery, followed by a dietary butyrate intervention for 7 weeks. Again, in the sham-operated group, butyrate reduced cumulative food intake (online supplementary figure S2A) as well as average food intake per se (online supplementary figure S2B) during the 7-week intervention period, and accelerated the clearance of [^{3}H]TO from the circulation (online supplementary figure S2C) as well as increased the uptake of [^{3}H]TO-derived activity by BAT (online supplementary figure S2D). Also, in mice receiving sham surgery, butyrate reduced iBAT pad weight (online supplementary figure S2E) most likely due to a decrease in intracellular lipid vacuole content (online supplementary figure S2F) and enhanced BAT thermogenic capacity as shown by an increased UCP-1 protein content (online supplementary figure S2G). However, after the subdiaphragmatic vagotomy, butyrate failed to reduce the cumulative food intake (figure 6A), and the average food intake *per se* between the control group and butyrate-treated group was equal (figure 6B). In vagotomised mice, butyrate treatment also did not influence the clearance of [^{3}H]TO from the circulation (figure 6C), nor the tissue uptake of [^{3}H]TO-derived activity (figure 6D). The weight of iBAT (figure 6E), the intracellular lipid vacuole content of iBAT (figure 6F) and UCP-1 protein content in iBAT (figure 6G) in the vagotomised mice received butyrate treatment that was comparable to that of control group. Taken together, these data indicate that the gut-brain neural circuit is necessary for the beneficial effects of butyrate on both satiety and BAT activation.

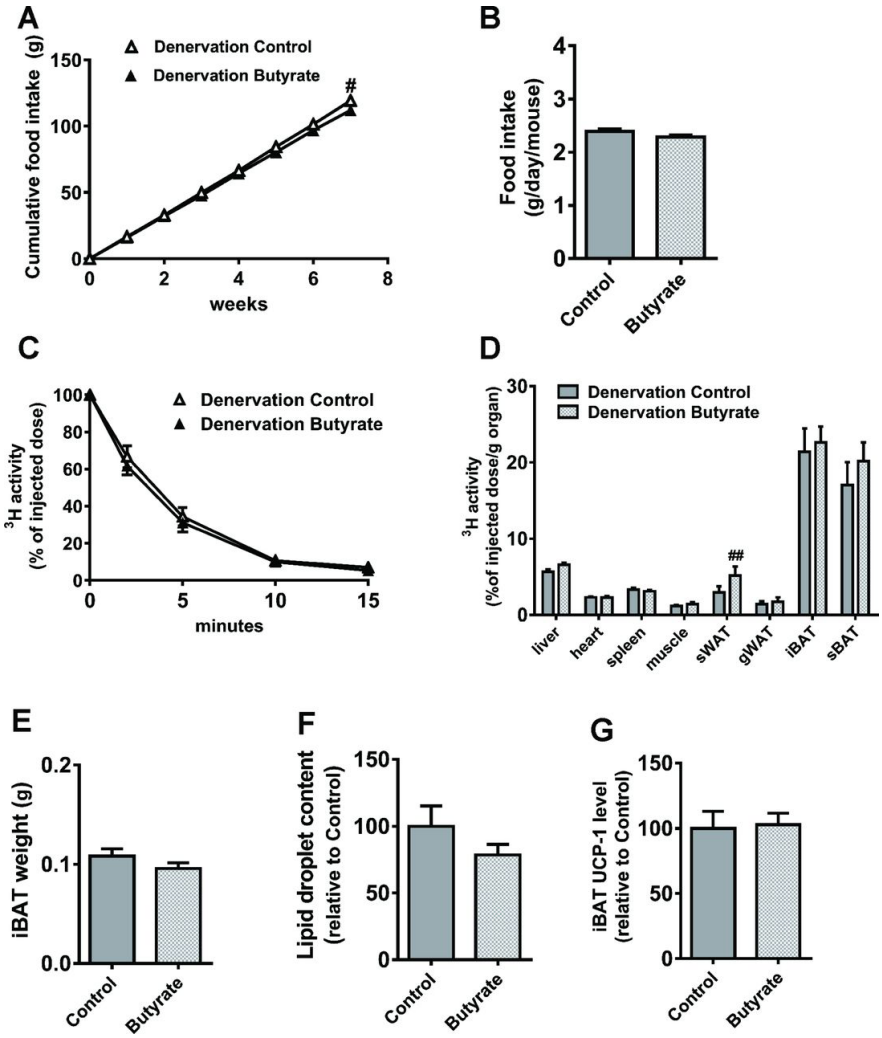

Figure 6. The gut-brain neural circuit is necessary for the butyrate-induced satiety and brown adipose tissue (BAT) activation. Mice were individually housed and received the subdiaphragmatic vagotomy surgery. One week after the surgery, mice were fed a high-fat diet (HFD) without (denervation control) or with 5% (w/w) sodium butyrate (denervation butyrate) for 7 weeks. Food intake was measured weekly and cumulative food intake (A) and average food intake *per se* (B) were calculated. At the end of this study, a triglyceride (TG) clearance test by intravenous injection of [^{3}H]TO-labelled TRL-like particles was performed. The clearance of [^{3}H]TO from the circulation (C) and uptake of ^{3}H by various tissue (D) was assessed. The weight of iBAT pad (E) was measured and the lipid content within the iBAT was quantified after the H&E staining (F). The protein expression of UCP-1 in iBAT was quantified after immunohistochemistry (IHC) of UCP-1 (G). Data are means ± SEM (n=8-9); #P<0.05 compared with denervation control. gWAT, gonadal white adipose tissue; iBAT, interscapular BAT; sBAT, subscapular BAT; sWAT, subcutaneous white adipose tissue; UCP, uncoupling protein.

Butyrate consumption alters gut microbiota composition

To investigate whether dietary butyrate affects the composition of gut microbiota, total bacterial DNA was isolated from the cecum content of sham-operated mice and vagotomised mice, after 7 weeks of butyrate treatment. The 16S rRNA gene was sequenced using the MiSeq platform. In sham-operated mice, dietary butyrate did not influence the number of observed species and the Shannon diversity index of the gut microbiota (figure 7A). However, unweighted UniFrac distance analysis showed a clear separation between control mice and butyrate-treated mice (figure 7B). As compared with control mice, butyrate-treated mice had a relative increased abundance of the phylum *Firmicutes* at the expense of *Bacteroidetes* (figure 7C). Linear discriminant analysis effect size indicated that genera belonging to the phylum *Firmicutes*, class *Erysipelotrichi* were significantly increased in butyrate-treated mice (figure 7D, E). Interestingly, in vagotomised mice, dietary butyrate significantly increased the number of observed species and the Shannon diversity index of the gut microbiota (online supplementary figure S5A). Unweighted UniFrac distance analysis showed a moderate separation between control mice and butyrate-treated vagotomised mice (online supplementary figure S5B). Similar to the effect in non-vagotomised mice, butyrate also increased the relative abundance of the phylum *Firmicutes* (online supplementary figure S5C), with even more classes affected, including *Erysipelotrichi*, *Clostridia* and *Bacilli* (online supplementary figure S5D, E). Collectively, our data clearly indicate that dietary butyrate alters the caecal microbiota composition, and in particular increasing the abundance of the phylum *Firmicutes*, independent of the presence of an intact gut-brain neural circuit.

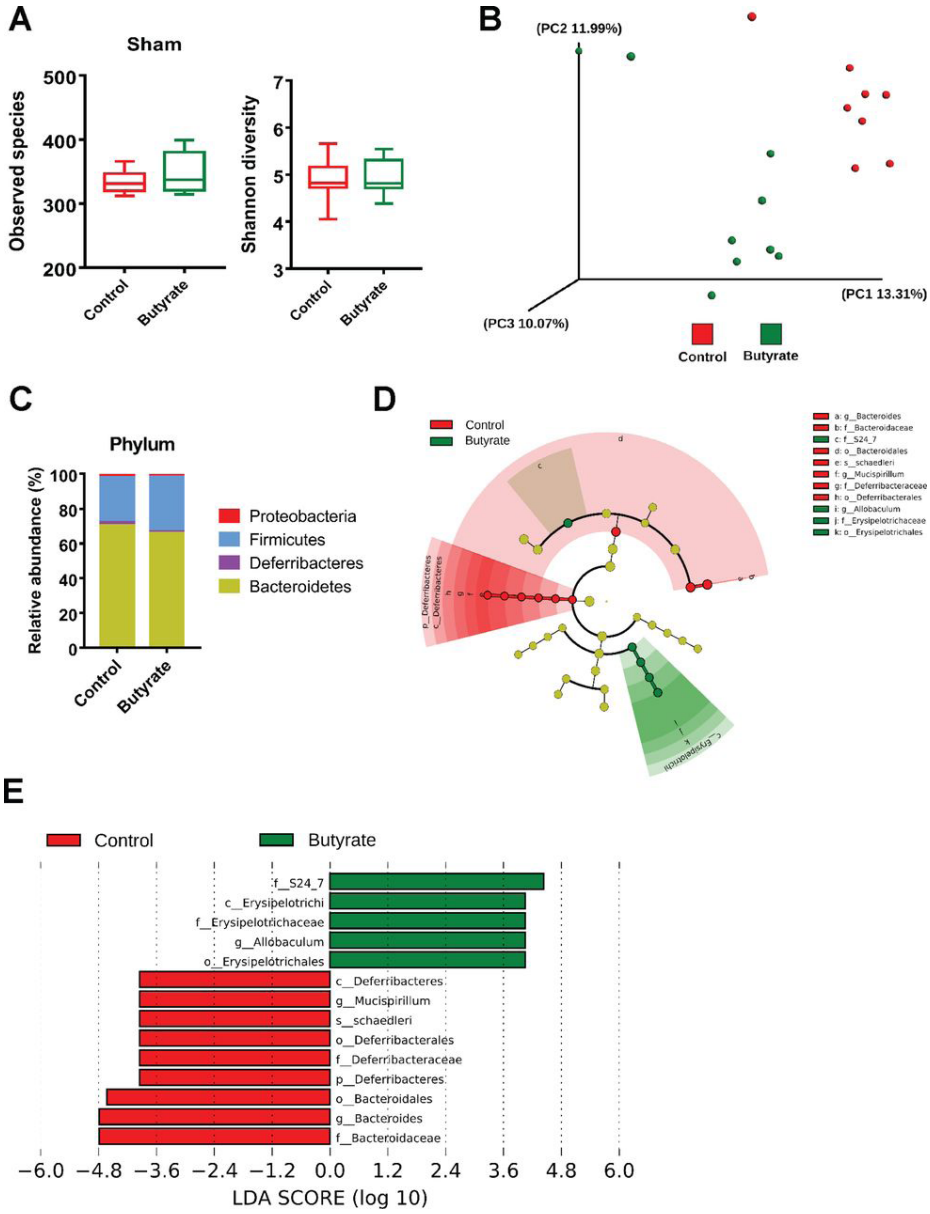

Figure 7. Butyrate consumption alters gut microbiota composition. After 7 weeks of intervention, total bacterial DNA was isolated from the caecum content and 16S rRNA genes were sequenced. (A) The number of observed species and the Shannon diversity of the gut microbiota. (B) Principal coordinates analysis plot of unweighted UniFrac distances. Composition of abundant bacterial phyla (C), cladogram generated from linear discriminant analysis (LDA) effect size (LEfSe) (D) and the LDA score (E) showing the most differentially significant abundant taxa enriched in microbiota from the control (red, n=8) and butyrate (green, n=9) group.

Discussion

Previous findings showed that both dietary administration of butyrate [13, 24] and stimulation of intestinal butyrate production via probiotics [25, 26] exert multiple beneficial effects on non-alcoholic fatty liver disease and energy metabolism. However, the mechanisms underlying the regulation of energy homeostasis by butyrate are still under debate. In this study, we showed that butyrate reduces food intake. This effect contributes dominantly to the various metabolic benefits of butyrate, including preventing HFD-induced obesity, fat mass gain and hepatic steatosis, and improving hyperglycemia and insulin resistance. In addition, butyrate also modestly promotes the oxidation of TG, likely by enhancing TG uptake by BAT activation during daytime.

In the search for mechanisms underlying the beneficial effects of butyrate on metabolism, we first demonstrated that both acute and chronic butyrate administration reduce food intake. Previous preclinical studies [27, 28] and clinical studies [17, 18] have demonstrated that administration of dietary fiber, a main resource for intestinal SCFA production by the gut microbiota, increases satiety and decreases energy intake, accompanied by increased endogenous butyrate production. However, the effect of butyrate per se on satiety was still under debate. den Besten *et al* [16] showed that 5% butyrate (w/w) incorporated into an HFD, in which 45% of calories were from palm oil fat, did not alter food intake in mice. In contrast, Lin *et al* [11] reported that 5% butyrate incorporated into another type of HFD in which 60% of calories were derived from lard and soybean oil, led to a 22% reduction in cumulative food intake over 9 days. We confirmed this finding by using the same lard fat in the diet, showing that 5% butyrate supplementation reduces cumulative food intake by 22% over a 9-week intervention period, without influencing spontaneous physical activity of the mice. These data suggest that butyrate unlikely induces systemic toxicity and abnormal motor and behavior at this dose. Further behavioral assays, including the conditional aversion assay, would be needed to firmly establish whether mice have aversion to butyrate due to its odor and/or taste. The discrepancy between studies may be attributed to the fact that the different dietary fat and carbohydrates distinctly impact the composition of the gut microbiota as well as the production of endogenous SCFAs, especially butyrate [29], therefore interfering with the satiety effect induced by exogenous butyrate. Of note, in chow-fed mice, butyrate administration via intragastric gavage rapidly induces satiety and prevented refeeding after an overnight fast. This finding suggests that independent of dietary composition and intestinal SCFAs, butyrate *per se* induces satiety and reduces cumulative food intake.

The GI tract is intimately connected to the central nervous system (CNS) mainly via hormonal and neuronal pathways, with the vagal nerve as the key neural connection between the GI tract and the CNS [30]. Our findings that reduced food intake coincided with reduced orexigenic NPY neuron activity in the hypothalamus, and decreased neuron activity within the NTS and DVC in the brainstem, indicate that

the effect of butyrate on satiety is likely mediated via vagal inputs to NPY neurons. Indeed, we observed that subdiaphragmatic vagotomy completely abolished the butyrate-induced satiety. It is known that the central terminals of vagal nerve innervate the brainstem, where vagal nerve transmission such as energy status signal projects to the hypothalamus, thereby forming a circuit to regulate satiety [31]. Due to our finding that direct intravenous infusion of butyrate did not affect food intake, hypothalamic neuronal sensing of energy status might be a primary target for butyrate supplementation.

On the other hand, the GI tract releases a number of gut hormones, including glucagon-like peptide 1 (GLP-1), which primarily acts on the vagal nerve and also travels through the circulation to directly act on the hypothalamus to regulate satiety signaling. In fact, several studies showed that oral butyrate has the capacity to stimulate GLP-1 secretion [11, 32]. Convincing evidence shows that GLP-1 receptor activation in vagal afferents [33] regulates food intake and energy metabolism. Collectively, it is tempting to speculate that butyrate consumption stimulates GLP-1 secretion from L cells of the GI tract, which activates GLP-1 receptor signaling in the vagal nerve and consequently induces hypothalamic satiety signaling. In addition, another important function of the gut-brain neural circuit is to regulate the intestinal transit [34], which plays an important role in nutrient harvest, thereby directly influencing host energy metabolism. A previous study has shown that butyrate increases colonic motility [35]. This may contribute to the metabolic benefits of butyrate by reducing nutrient absorption. Furthermore, Wichmann *et al* demonstrated that gut microbiota regulate intestinal transit via modulating GLP-1 production [36]. In the present study, it remains to be determined to what extent intestinal transit time and motility play a role in the beneficial effects of butyrate. By adding a pair-fed group, we could show that the reduced food intake is the dominant mechanism responsible for multiple distal beneficial effects of butyrate, including preventing diet-induced hepatic steatosis and hyperglycemia. The effects of butyrate on body weight and fat mass gain, plasma TG and insulin sensitivity were only partly (60%–70%) explained by reduction of food intake.

In addition to inducing satiety, butyrate also promoted the oxidation of fatty acids at the expense of carbohydrates, in particular during conditions of reduced feeding at daytime. An increase in fatty acid oxidation is characteristic for BAT activation [37] and we have previously reported a similar metabolic shift from glucose to lipid oxidation after central administration of the GLP-1 receptor agonist exendin-4 [38]. Therefore, it was not unexpected to find that butyrate accelerates the clearance of plasma TG by activated BAT. BAT functionality is primarily driven by hypothalamus via the action of the SNS [8]. We speculate that dietary butyrate reaching the GI tract most likely activates the gut-brain neural circuit, thereby stimulating hypothalamic control of the SNS outflow towards BAT. Consequently, butyrate activates BAT and increases oxidation of intracellular fatty acids resulting in a compensatory influx of TG-derived fatty acids. In fact, butyrate increased in BAT the protein level of TH, which is a marker of SNS activity [39]. In vagotomised

mice, butyrate failed to increase the uptake of TG-derived fatty acids by BAT, the utilization of lipid in BAT as well as the protein level of UCP-1, a positive marker for BAT activation. Butyrate also increased the flux of TG-derived fatty acids and glucose into WAT, at least per gram tissue, but did not induce browning of WAT. Since butyrate markedly decreased the size of adipocyte in WAT (online supplementary figure S3C, D), thereby increasing the number of adipocytes per gram tissue, butyrate probably does not affect the uptake capacity of white adipocytes *per se*. Although the relative volume of BAT in humans may be limited compared with skeletal muscle, the uptake of fatty acids per gram tissue by BAT exceeds that by skeletal muscle by >10-fold (figure 3F). Also, a recent paper redefined whole-body BAT distribution in humans and concluded that its metabolic capacity is substantially higher than usually reported [40]. The effects of butyrate on fatty acid uptake and oxidation by BAT we observe in mice may thus well be relevant for humans.

In addition to butyrate, administration of other SCFAs has been reported to induce satiety [41, 42]. Like butyrate, propionate induces satiety in ruminants probably also via the action of the vagal nerve [43], while acetate may directly regulate hypothalamic satiety signaling after crossing the blood–brain barrier [42]. Notably, a recent study showed that an increased production of intestinal acetate due to a high fat-diet feeding led to the development of obesity and insulin resistance through activation of the vagal nerve [44]. This suggests that dietary acetate acts differently on energy metabolism compared with acetate derived from intestinal bacteria fermentation. In this study, dietary butyrate clearly altered the caecal microbiota composition and increased the abundance of the phylum *Firmicutes*. Previously, increased abundance of the phylum *Firmicutes* has been associated with a less beneficial metabolic profile [45]. However, the specific species amplified within this phylum by butyrate may beneficially affect host energy metabolism. Future studies are needed to investigate the specific contribution of the altered gut microbiota to the beneficial effects of butyrate on host energy metabolism, for example, via fecal microbiota transplantation.

Undoubtedly, weight loss-enhancing strategies are among the most effective interventions for obesity-related diseases, that is, diabetes and cardiovascular disease. Body weight loss can be achieved by decreasing energy intake, that is, decreasing the consumption or absorption of food, and/or by increasing energy expenditure. Although bariatric surgery results in clinically significant weight loss and other beneficial effects, it suffers from a number of adverse events, including surgical complications, perioperative technical outcomes and mortality [46, 47]. Several antiobesity agents have been developed and are clinically applied with significant benefits, but do have a high probability of developing adverse effects, in particular in the application for long-term weight management [10]. Butyrate is currently widely emerging as a potential strategy for treatment of cancer, IBD, inherited disorders and neurodegeneration [48]. Our collective data now show that butyrate also induces sustained satiety and enhances fat oxidation, thereby effectively preventing diet-induced obesity, insulin resistance, hypertriglyceridemie

and hepatic steatosis, without inducing any apparent unfavorable effects. Therefore, we propose oral butyrate administration as a promising strategy to combat obesity and related cardiometabolic diseases.

References

1. Grundy, S.M., *Metabolic syndrome update.* Trends Cardiovasc Med, 2016. **26**(4): p. 364-73.
2. Schoeller, D.A., *Insights into energy balance from doubly labeled water.* Int J Obes (Lond), 2008. **32 Suppl 7**: p. S72-5.
3. Cypess, A.M., et al., *Identification and importance of brown adipose tissue in adult humans.* N Engl J Med, 2009. **360**(15): p. 1509-17.
4. van Marken Lichtenbelt, W.D., et al., *Cold-activated brown adipose tissue in healthy men.* N Engl J Med, 2009. **360**(15): p. 1500-8.
5. Cypess, A.M. and C.R. Kahn, *Brown fat as a therapy for obesity and diabetes.* Curr Opin Endocrinol Diabetes Obes, 2010. **17**(2): p. 143-9.
6. Schilperoort, M., et al., *Relevance of lipid metabolism for brown fat visualization and quantification.* Curr Opin Lipidol, 2016. **27**(3): p. 242-8.
7. Labbe, S.M., et al., *Hypothalamic control of brown adipose tissue thermogenesis.* Front Syst Neurosci, 2015. **9**: p. 150.
8. Kooijman, S., J.K. van den Heuvel, and P.C.N. Rensen, *Neuronal Control of Brown Fat Activity.* Trends Endocrinol Metab, 2015. **26**(11): p. 657-668.
9. Ahima, R.S. and D.A. Antwi, *Brain regulation of appetite and satiety.* Endocrinol Metab Clin North Am, 2008. **37**(4): p. 811-23.
10. Apovian, C.M., W.T. Garvey, and D.H. Ryan, *Challenging obesity: Patient, provider, and expert perspectives on the roles of available and emerging nonsurgical therapies.* Obesity (Silver Spring), 2015. **23 Suppl 2**: p. S1-S26.
11. Lin, H.V., et al., *Butyrate and propionate protect against diet-induced obesity and regulate gut hormones via free fatty acid receptor 3-independent mechanisms.* PLoS One, 2012. **7**(4): p. e35240.
12. Khan, S. and G. Jena, *Sodium butyrate reduces insulin-resistance, fat accumulation and dyslipidemia in type-2 diabetic rat: A comparative study with metformin.* Chem Biol Interact, 2016. **254**: p. 124-34.
13. Gao, Z., et al., *Butyrate improves insulin sensitivity and increases energy expenditure in mice.* Diabetes, 2009. **58**(7): p. 1509-17.
14. Mattace Raso, G., et al., *Effects of sodium butyrate and its synthetic amide derivative on liver inflammation and glucose tolerance in an animal model of steatosis induced by high fat diet.* PLoS One, 2013. **8**(7): p. e68626.
15. Henagan, T.M., et al., *Sodium butyrate epigenetically modulates high-fat diet-induced skeletal muscle mitochondrial adaptation, obesity and insulin resistance through nucleosome positioning.* Br J Pharmacol, 2015. **172**(11): p. 2782-98.
16. den Besten, G., et al., *Short-Chain Fatty Acids Protect Against High-Fat Diet-Induced Obesity via a PPARgamma-Dependent Switch From Lipogenesis to Fat Oxidation.* Diabetes, 2015. **64**(7): p. 2398-408.

17. Cani, P.D., et al., *Oligofructose promotes satiety in healthy human: a pilot study.* Eur J Clin Nutr, 2006. **60**(5): p. 567-72.

18. Daud, N.M., et al., *The impact of oligofructose on stimulation of gut hormones, appetite regulation and adiposity.* Obesity (Silver Spring), 2014. **22**(6): p. 1430-8.

19. van den Hoek, A.M., et al., *APOE*3Leiden.CETP transgenic mice as model for pharmaceutical treatment of the metabolic syndrome.* Diabetes Obes Metab, 2014. **16**(6): p. 537-44.

20. van den Maagdenberg, A.M., et al., *Transgenic mice carrying the apolipoprotein E3-Leiden gene exhibit hyperlipoproteinemia.* J Biol Chem, 1993. **268**(14): p. 10540-5.

21. Wang, Y., et al., *Plasma cholesteryl ester transfer protein is predominantly derived from Kupffer cells.* Hepatology, 2015. **62**(6): p. 1710-22.

22. Wieczorek, M., et al., *Physiological and behavioral responses to interleukin-1beta and LPS in vagotomized mice.* Physiol Behav, 2005. **85**(4): p. 500-11.

23. Rensen, P.C., et al., *Selective liver targeting of antivirals by recombinant chylomicrons--a new therapeutic approach to hepatitis B.* Nat Med, 1995. **1**(3): p. 221-5.

24. Jin, C.J., et al., *Supplementation of sodium butyrate protects mice from the development of non-alcoholic steatohepatitis (NASH).* Br J Nutr, 2015. **114**(11): p. 1745-55.

25. Yadav, H., et al., *Beneficial metabolic effects of a probiotic via butyrate-induced GLP-1 hormone secretion.* J Biol Chem, 2013. **288**(35): p. 25088-97.

26. Endo, H., et al., *Butyrate-producing probiotics reduce nonalcoholic fatty liver disease progression in rats: new insight into the probiotics for the gut-liver axis.* PLoS One, 2013. **8**(5): p. e63388.

27. Cani, P.D., et al., *Oligofructose promotes satiety in rats fed a high-fat diet: involvement of glucagon-like Peptide-1.* Obes Res, 2005. **13**(6): p. 1000-7.

28. Kleessen, B., L. Hartmann, and M. Blaut, *Oligofructose and long-chain inulin: influence on the gut microbial ecology of rats associated with a human faecal flora.* Br J Nutr, 2001. **86**(2): p. 291-300.

29. Jurgonski, A., J. Juskiewicz, and Z. Zdunczyk, *A high-fat diet differentially affects the gut metabolism and blood lipids of rats depending on the type of dietary fat and carbohydrate.* Nutrients, 2014. **6**(2): p. 616-26.

30. Chaudhri, O.B., et al., *Gastrointestinal satiety signals.* Annu Rev Physiol, 2008. **70**: p. 239-55.

31. Schneeberger, M., R. Gomis, and M. Claret, *Hypothalamic and brainstem neuronal circuits controlling homeostatic energy balance.* J Endocrinol, 2014. **220**(2): p. T25-46.

32. Tolhurst, G., et al., *Short-chain fatty acids stimulate glucagon-like peptide-1 secretion via the G-protein-coupled receptor FFAR2.* Diabetes, 2012. **61**(2): p. 364-71.

33. Krieger, J.P., et al., *Knockdown of GLP-1 Receptors in Vagal Afferents Affects Normal Food Intake and Glycemia.* Diabetes, 2016. **65**(1): p. 34-43.

34. Ciesielczyk, K., et al., *Altered sympathovagal balance and pain hypersensitivity in TNBS-induced colitis.* Arch Med Sci, 2017. **13**(1): p. 246-255.

35. Soret, R., et al., *Short-chain fatty acids regulate the enteric neurons and control gastrointestinal motility in rats.* Gastroenterology, 2010. **138**(5): p. 1772-82.

36. Wichmann, A., et al., *Microbial modulation of energy availability in the colon regulates intestinal transit.* Cell Host Microbe, 2013. **14**(5): p. 582-90.

37. Berbee, J.F., et al., *Brown fat activation reduces hypercholesterolaemia and protects from atherosclerosis development.* Nat Commun, 2015. **6**: p. 6356.

38. Kooijman, S., et al., *Central GLP-1 receptor signalling accelerates plasma clearance of triacylglycerol and glucose by activating brown adipose tissue in mice.* Diabetologia, 2015. **58**(11): p. 2637-46.

39. Schmidt, R.E. and B.E. Cogswell, *Tyrosine hydroxylase activity in sympathetic nervous system of rats with streptozocin-induced diabetes.* Diabetes, 1989. **38**(8): p. 959-68.

40. Leitner, B.P., et al., *Mapping of human brown adipose tissue in lean and obese young men.* Proc Natl Acad Sci U S A, 2017. **114**(32): p. 8649-8654.

41. Farningham, D.A. and C.C. Whyte, *The role of propionate and acetate in the control of food intake in sheep.* Br J Nutr, 1993. **70**(1): p. 37-46.

42. Frost, G., et al., *The short-chain fatty acid acetate reduces appetite via a central homeostatic mechanism.* Nat Commun, 2014. **5**: p. 3611.

43. Anil, M.H. and J.M. Forbes, *The roles of hepatic nerves in the reduction of food intake as a consequence of intraportal sodium propionate administration in sheep.* Q J Exp Physiol, 1988. **73**(4): p. 539-46.

44. Perry, R.J., et al., *Acetate mediates a microbiome-brain-beta-cell axis to promote metabolic syndrome.* Nature, 2016. **534**(7606): p. 213-7.

45. Turnbaugh, P.J., et al., *An obesity-associated gut microbiome with increased capacity for energy harvest.* Nature, 2006. **444**(7122): p. 1027-31.

46. Maggard-Gibbons, M., et al., *Bariatric surgery for weight loss and glycemic control in nonmorbidly obese adults with diabetes: a systematic review.* JAMA, 2013. **309**(21): p. 2250-61.

47. Hopkins, J.C., et al., *Outcome reporting in bariatric surgery: an in-depth analysis to inform the development of a core outcome set, the BARIACT Study.* Obes Rev, 2015. **16**(1): p. 88-106.

48. Berni Canani, R., M. Di Costanzo, and L. Leone, *The epigenetic effects of butyrate: potential therapeutic implications for clinical practice.* Clin Epigenetics, 2012. **4**(1): p. 4.

Supplementary materials and methods

Appetite test and brain histology

After overnight fasting (7pm-8am), mice were randomized based on body weight and received sodium butyrate or vehicle by intra-gastric gavage (6 M, 0.15 mL per mouse) or intravenous injection (15 mM or 150 mM, 0.1 mL per mouse). Food intake per se was measured during the next 24 hours. In a second experiment, 1 hour after intra-gastric gavage of sodium butyrate or vehicle, mouse brains were collected for histological analysis.

Hypothalamic histology

- C-FOS immunohistochemistry in hypothalamus

One hour after intra-gastric gavage of sodium butyrate or vehicle, mice were anesthetized and perfused transcardially with ice-cold saline followed by freshly prepared 4% paraformaldehyde solution. The brains were collected, postfixed in 4% paraformaldehyde for 48 hours, cryoprotected in 30% sucrose and subsequently frozen on dry ice and stored at −80°C. Thirty-five µm-cryostat sections of frozen brains were cut and stored in cryoprotectant at -20°C.

c-FOS immunohistochemistry was performed on serial hypothalamic sections cut from -1.22 mm to -1.70 mm relative to the bregma according to The Mouse Brain in Stereotaxic Coordinates. Brain sections were blocked by 2% normal goat serum (NGS) and incubated with anti-c-Fos primary antibody (1:1000, Abcam), Alexa 594 secondary goat anti-rabbit antibody (1:500, Abcam) and diaminobenzidine (DAB) and DAPI as chromogen (SK-4100, Vector laboratories). The quantification of c-FOS-positive cells within the arcuate nucleus (3-4 sections per mouse) were determined using Image J software system.

- Double immunofluorescent staining

Double immunofluorescent staining of c-Fos with POMC or NPY were performed on the same serial hypothalamic sections as described above. Brain sections were incubated with primary antibodies: goat anti-c-Fos (1:500, Santa Cruz), and rabbit anti-POMC (1:800, Phoenix Pharmaceuticals), or rabbit anti-NPY (1:500, Abcam), respectively, at 4 °C overnight. Sections were rinsed and incubated with biotinylated secondary anti-goat or anti-rabbit IgG for 1 h, and then rinsed and incubated with streptavidin-conjugated Alexa Fluor® 594 or 647 (Jackson ImmunoResearch, USA) for 1 h. All sections were then rinsed and mounted on gelatin-coated glass slides, dried, covered with polyvinyl alcohol mounting medium containing DABCO® (Sigma, USA), observed and imaged by confocal microscopy (Leica SP8, Germany). The quantification of colocalization percentage of NPY-positive neurons or POMC-positive neurons that coexpress c-FOS within the arcuate nucleus were determined using Image J software system.

Neuron activity in brain regions of cortex, hippocampus, brainstem

c-FOS immunohistochemistry was performed on serial hypothalamic sections cut from -1.22 mm to −1.70 mm, and brainstem sections cut from -7.32 mm to -7.76 mm relative to the bregma according to The Mouse Brain in Stereotaxic Coordinates. Sections were incubated with anti-c-Fos primary antibody (1:1000, Abcam), biotinylated secondary anti-rabbit IgG, avidin-biotin complex (ABC method, Vector Laboratories, Inc., Burlingame, CA), and the reaction product was visualized by incubation in 1% diaminobenzidine with 0.01% hydrogen peroxide. The quantification of c-FOS-positive cells in cortical regions (primary somatosensory cortex and primary and secondary motor cortex), hippocampal regions, nucleus tractus solitarius (NTS) and dorsal vagal complex (DVC) within brainstem were determined using Image J software system.

Short chain fatty acid measurement by the gas chromatography–mass spectrometry (GC-MS)

Plasma short chain fatty acids were analyzed by GC-MS using previously published approach with some modifications [1]. Briefly, 10 µL of plasma was transferred to a glass vial containing 250 µL acetone (Sigma-Aldrich), 10 µL 1 ppm internal standards solution containing acetic acid-d4, propionic acid-6 and butyric acid-d8 (Sigma Aldrich) and 10 µL ethanol. Thereafter, samples were derivatized with pentafluorobenzyl bromide (PFBBr), as follows: 100 µL 172 mM PFBBr (Thermo) in acetone was added, samples were mixed and heated to 60 ˚C for 30 min. After the samples had cooled down to room temperature a liquid-liquid extraction was performed using 500 µL n-hexane (Sigma-Aldrich) and 250 µL GC-MS grade water. The upper n-hexane layer was transferred to a fresh glass vial and subsequently used for GC-MS analysis. Calibration standards were prepared analogous. For calibration standards no plasma was added and 10 µL of EtOH was replaced by 10 µL standards solution (Sigma-Aldrich) in EtOH.

Samples were analyzed on a Bruker Scion 436 GC fitted with an Agilent VF-5ms capillary column (25m × 0.25mm i.d.,0.25 µm film thickness) coupled to a Bruker Scion TQ MS. Injection was performed using a CTC PAL autosampler (G6501-CTC): 1 µL sample was injected splitless at 280˚C. Helium 99.9990% was used as carrier gas at a constant flow of 1.20 mL/min. The GC temperature program was set as follows: 1 min. constant at 50˚C, then linear increase at 40˚C/min to 60˚C, kept constant for 3 min, followed by a linear increase at 25˚C/min to 200˚C, linearly increased at 40˚C/min to 315˚C, kept constant for 2 min. The transfer line and ionization source temperature were 280˚C. The pressure of the chemical ionization gas, methane (99.9990%), was set at 15 psi. Negatively charged ions were detected in the selected ion monitoring mode, and acetic acid, acetic acid-d4, propionic acid, propionic acid-d6, butyric acid and butyric acid-d8 were monitored at m/z 59, 62, 73, 78, 87 and 94 respectively.

Body weight and body composition

Body weight was measured with a scale, and body composition was measured in conscious mice using an EchoMRI-100 analyzer (EchoMRI, Houston, TX).

Hepatic lipid content

Liver lipids were extracted according to a modified protocol from Bligh and Dyer [2]. Small liver pieces (approx. 30 mg) were homogenized in ice-cold methanol. By addition of CH_3OH:$CHCl_3$ (1:3 v/v) to the homogenate, followed by vigorous vortexing and phase separation by centrifugation, lipids were extracted into the $CHCl_3$ phase. Subsequently, the lipid phase was dried and dissolved in 2% Triton X-100. TG, total cholesterol (TC) and phospholipid (PL) concentrations were measured using the commercial kits 11488872, 236691 (Roche Molecular Biochemicals) and phospholipids B (Wako Chemicals), respectively. Hepatic lipid content was expressed as nmol lipid per mg protein, which was determined using the BCA protein assay kit (Pierce).

Plasma parameters

After a 5-h fasting period (8am-1pm), blood was obtained via tail vein bleeding into heparin-coated capillary tubes just before the sodium butyrate supplementation and at the end of the intervention. The capillary tubes were placed on ice and centrifuged, and obtained plasma was snap-frozen in liquid nitrogen and stored at -80°C until further measurements. Plasma was assayed for TG, glucose and insulin using commercially available kits as described previously [3]. The homeostasis model index of insulin (HOMA-IR) as an index for insulin resistance was calculated by multiplying fasting insulin (mU/L) with fasting glucose (nmol/L), and dividing by 22.5 [4].

***In vivo* lipid and glucose clearance**

Triacylglycerol-rich lipoprotein (TRL)-like particles (average size of 80 nm) labeled with glycerol tri[^{3}H]oleate (triolein, [^{3}H]TO) were prepared and mixed with 2-[1-^{14}C] deoxy-D-glucose ([^{14}C]DG) in a 3:1 ratio based on radioactive counts. Particles were stored at 4°C under argon and used for in vivo kinetic experiments.

At 9.00 am, mice were injected with 200 µL of emulsion particles (1 mg TG) and [^{14}C]DG via the tail vein at the end of the intervention period. Blood samples were taken at 2, 5, 10 and 15 min after injection, and lipid and glucose clearance kinetics were determined by measuring plasma ^{3}H and ^{14}C activities. After 15 min, mice were sacrificed by cervical dislocation and perfused with ice-cold saline via the heart. Thereafter, organs were harvested and weighed and dissolved overnight at 60°C in a Tissue Solubilizer (Amersham Biosciences, Roosendaal, the Netherlands). The uptake of [^{3}H]TO- and [^{14}C]DG-derived radioactivity by the organs was calculated

from the ^{3}H and ^{14}C activities in each organ and expressed as percentage of injected dose per gram wet tissue weight.

Indirect calorimetry

Indirect calorimetry was performed in fully automatic metabolic cages (LabMaster System, TSE Systems, Bad Homburg, Germany) in the first week of the intervention. After 2 days of acclimatization, O_2 consumption, CO_2 production and physical activity were measured for 3 consecutive days. The 5 average respiratory exchange ratio, energy expenditure, fat and carbohydrate oxidation rates were calculated as described previously [5].

BAT histology and TG content

Formalin-fixed paraffin-embedded interscapular BAT (iBAT) tissue sections (5 μm) were prepared for hematoxylin and eosin (H&E) staining using standard protocols, and stained for uncoupling protein-1 (UCP-1, 1/4000; Ab10983; Abcam) and tyrosine hydroxylase (TH, 1/2000; Ab112; Abcam) as described previously [6]. The areas occupied by intracellular lipid vacuoles, nuclear, UCP-1 and TH were quantified using Image J software (National Institutes of Health). The protein content of UCP-1 was expressed as positive area per total iBAT area, and the protein content of TH was expressed as positive area per cell nuclear area, which was represented the cell number.

WAT histology and adipocyte size

Formalin-fixed paraffin-embedded subcutaneous WAT (sWAT) and gonadal WAT (gWAT) sections (5 μm) were prepared for hematoxylin and eosin (H&E) staining using standard protocols, and stained for uncoupling protein-1 (UCP-1, 1/4000; Ab10983; Abcam). The average adipocyte size (μm2) was quantified per mouse using Image J software (National Institutes of Health), and normalized to Control group.

Microbiota analysis

After 7 weeks of butyrate treatment, total caecal bacterial DNA was isolated from cecum content in mice received subdiaphragmatic vagotomy surgery or sham surgery as described previously [7]. Microbial 16S rRNA gene was amplified targeting the hyper-variable region V4. Sequencing was performed using the Illumina MiSeq platform (BGI Genomics, Hong Kong) generating paired-end reads of 250 bp in length in each direction. Overlapping paired-end reads were subsequently aligned. Reads quality was checked with Sickle, version:1.33 (https://github.com/najoshi/sickle) and low quality reads were removed. For visualizing the taxonomic composition of the fecal microbiota and further beta diversity analysis, QIIME version: 1.9.1 was used [8]. In brief, closed reference operational taxonomic

unit (OTU) picking with 97% sequence similarity against GreenGenes 13.8 reference database was done. Jackknifed beta-diversity of unweighted UniFrac distances with 10 jackknife replicates was measured at rarefaction depth of 20000 reads / sample. For statistical significance, biological relevance and visualization we used linear discriminant analysis (LDA) effect size (LEfSe) method which uses standard parameters ($P<0.05$ and LDA score 2.0) as described in (https://bitbucket.org/biobakery/biobakery/wiki/lefse).

Supplemental figures

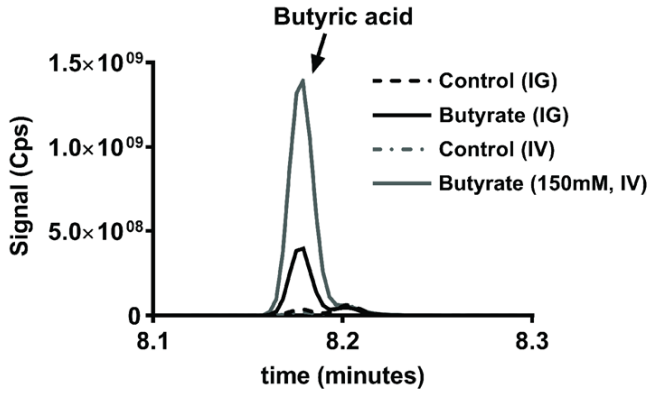

Figure S1. Oral and intravenous butyrate supplementation increases plasma butyrate concentration. After overnight fasting and randomization based on bodyweight, mice received vehicle or butyrate via the intra-gastric gavage (IG) or intravenous injection (IV). 1 hour after receiving butyrate, plasma were pooled for the measurement of butyrate level by GC-MS.

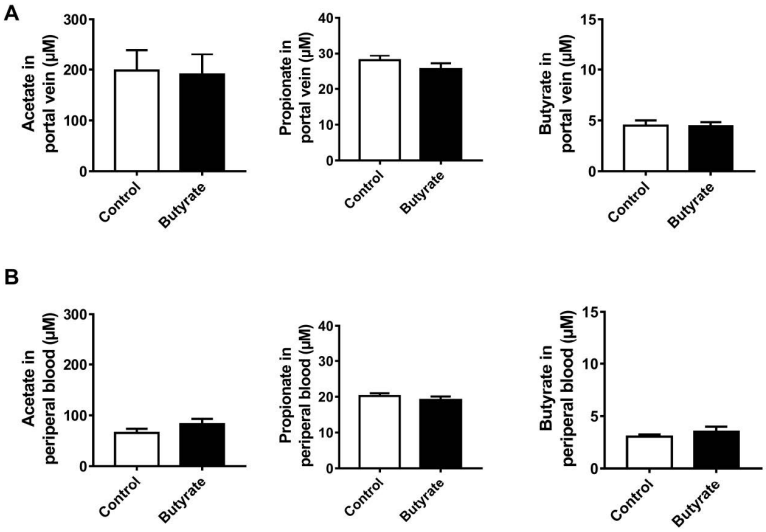

Figure S2. Chronic dietary butyrate consumption does not alter the levels of acetate, propionate and butyrate in portal vein or peripheral blood. Mice were individually housed and receive a HFD without (Control group), or with 5% (w/w) sodium butyrate (Butyrate group) for 9 weeks. At the end of this study, portal vein blood and peripheral blood were collected, the levels of acetate, propionate and butyrate were determined by GC-MS. Data are means ± SEM (n=6-7).

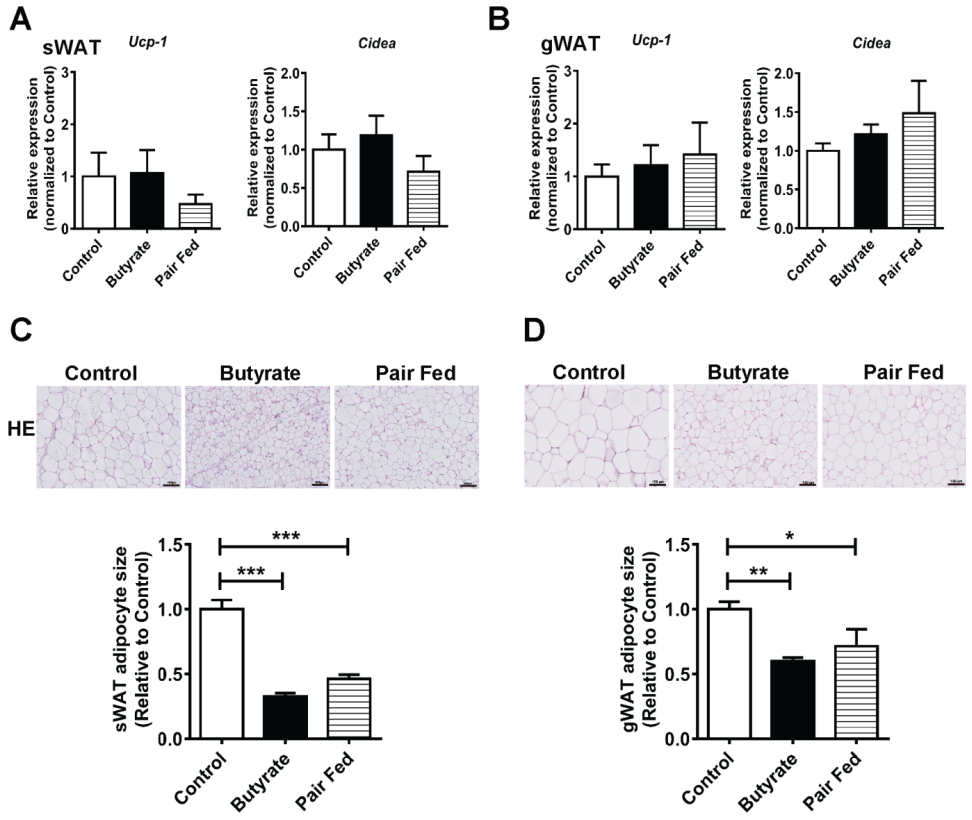

Figure S3. Butyrate treatment does not induce browning of white adipose tissue. After 9 weeks of intervention, the subcutaneous white adipose tissue (sWAT, A, C) and gonadal white adipose tissue (gWAT, B, D) were collected. mRNA expression of *Ucp-1* and *Cidea* were determined (A, B). Slides were stained for H&E, and the adipocyte size was quantified (C, D). Data are means ± SEM (n=8-9). *P<0.05, **P<0.01, ***P<0.001 as compared to control group.

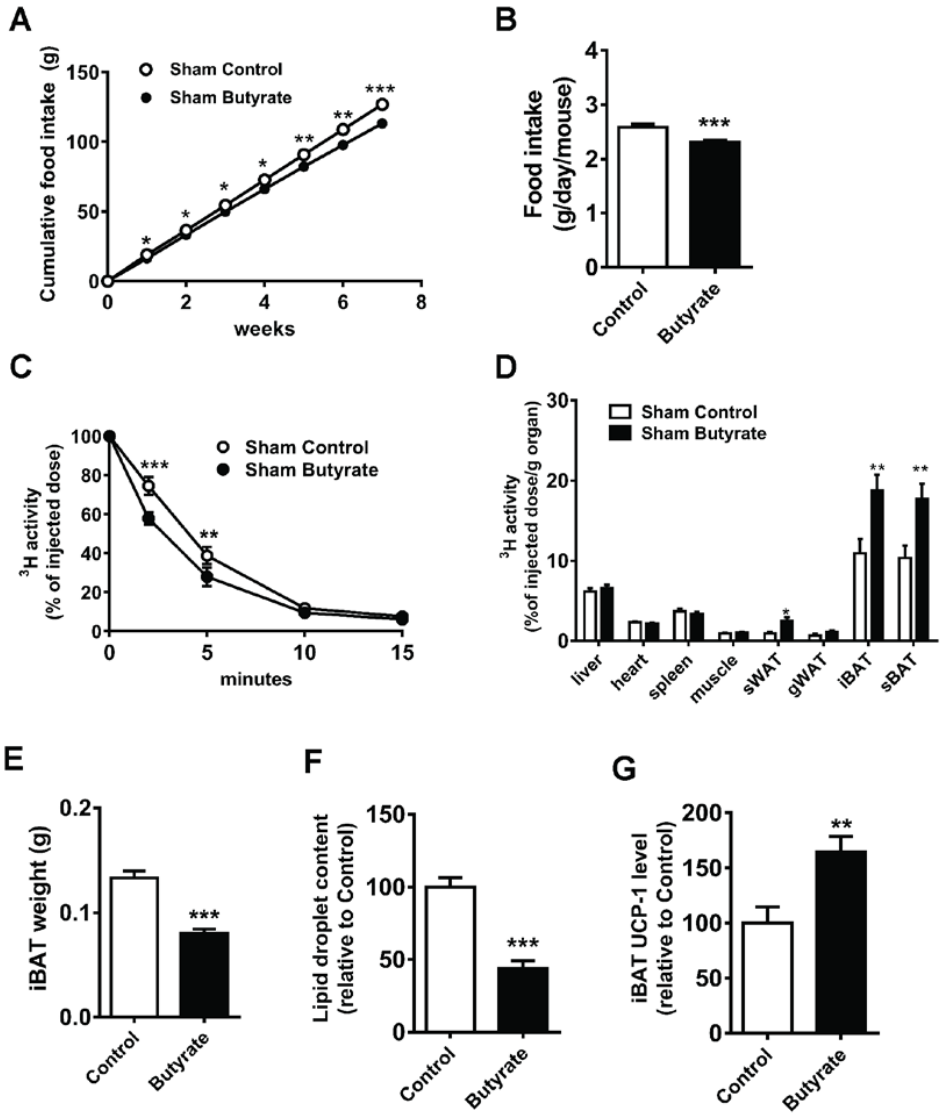

Figure S4. Butyrate decreases food intake and activates brown adipose tissue in mice received sham surgery (related to Figure 6). Mice were individually housed and received sham surgery. One week after the surgery, mice were fed a HFD without (Sham Control) or with 5% (w/w) sodium butyrate (Sham Butyrate) for 7 weeks. Food intake was measured weekly and cumulative food intake (A) and average food intake *per se* (B) was calculated. At the end of this study, a TG clearance test by i.v. injection of [^{3}H]TO-labeled TRL-like particles was performed. The clearance of [^{3}H]TO from the circulation (C) and uptake of ^{3}H by various tissue (D) was assessed. The weight of iBAT pad (E) was measured and the lipid content within the iBAT was quantified after the H&E staining (F). The protein expression of UCP-1 in iBAT was quantified after IHC of UCP-1 (G). Data are means ± SEM (n=8-9); *P<0.05, **P<0.01, ***P<0.001 compared to sham control.

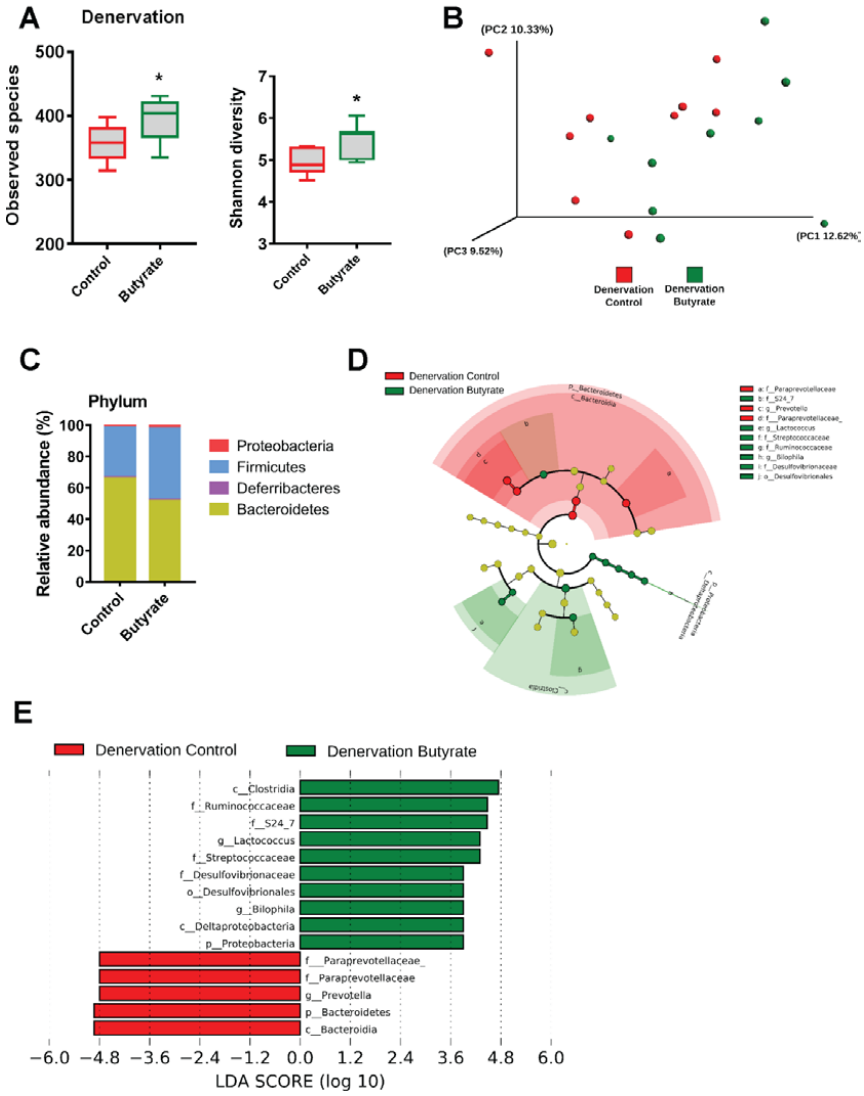

Figure S5. Butyrate consumption alters gut microbiota composition. After 7 weeks of intervention, total cecal bacterial DNA was isolated from the cecum content in mice received subdiaphragmatic vagotomy surgery and 16S rRNA genes were sequenced. (A) The α diversity including observed species and Shannon diversity of the gut microbiota. (B) Principal coordinates analysis plot of Unweighted Unifrac distances. Composition of abundant bacterial phyla (C), Cladogram generated from LEfSe analysis (D) and the LDA score (E) showing the most differentially significant abundant taxa enriched in microbiota from the denervation control (red) and denervation butyrate (green) group. For A, data was shown as Box& whiskers, Mann-Whitney test, *P<0.05 as compared to denervation control group.

Supplemental references

1. Tomcik, K., et al., *Isotopomer enrichment assay for very short chain fatty acids and its metabolic applications.* Anal Biochem, 2011. **410**(1): p. 110-7.
2. Bligh, E.G. and W.J. Dyer, *A rapid method of total lipid extraction and purification.* Can J Biochem Physiol, 1959. **37**(8): p. 911-7.
3. Wang, Y., et al., *Exendin-4 decreases liver inflammation and atherosclerosis development simultaneously by reducing macrophage infiltration.* Br J Pharmacol, 2014. **171**(3): p. 723-34.
4. Mather, K., *Surrogate measures of insulin resistance: of rats, mice, and men.* Am J Physiol Endocrinol Metab, 2009. **296**(2): p. E398-9.
5. Van Klinken, J.B., et al., *Estimation of activity related energy expenditure and resting metabolic rate in freely moving mice from indirect calorimetry data.* PLoS One, 2012. **7**(5): p. e36162.
6. Kooijman, S., et al., *Central GLP-1 receptor signalling accelerates plasma clearance of triacylglycerol and glucose by activating brown adipose tissue in mice.* Diabetologia, 2015. **58**(11): p. 2637-46.
7. Janssen, A.W.F., et al., *Modulation of the gut microbiota impacts nonalcoholic fatty liver disease: a potential role for bile acids.* J Lipid Res, 2017. **58**(7): p. 1399-1416.
8. Caporaso, J.G., et al., *QIIME allows analysis of high-throughput community sequencing data.* Nat Methods, 2010. **7**(5): p. 335-6.